

# On the nature of the ultraluminous X-ray transient in Cen A (NGC 5128)

Kajal K. Ghosh<sup>1</sup>, Mark H. Finger<sup>1</sup>, Douglas A. Swartz<sup>1</sup>, Allyn F. Tennant<sup>2</sup>, and Kinwah Wu<sup>3</sup>

## ABSTRACT

We combine 9 *ROSAT*, 9 *Chandra*, and 2 *XMM-Newton* observations of the Cen A galaxy to obtain the X-ray light curve of 1RXH J132519.8–430312 (=CXOU J132519.9–430317) spanning 1990 to 2003. The source reached a peak 0.1–2.4 keV flux  $F_X > 10^{-12}$  ergs cm<sup>-2</sup> s<sup>-1</sup> during a 10 day span in 1995 July. The inferred peak isotropic luminosity of the source therefore exceeded  $3 \times 10^{39}$  ergs s<sup>-1</sup>, which places the source in the class of ultra-luminous X-ray sources. Coherent pulsations at 13.264 Hz are detected during a second bright episode ( $F_X > 3 \times 10^{-13}$  ergs cm<sup>-2</sup> s<sup>-1</sup>) in 1999 December. The source is detected and varies significantly within three additional observations but is below the detection threshold in 7 observations. The X-ray spectrum in 1999 December is best described as a cut-off power law or a disk-blackbody (multi-colored disk). We also detect an optical source,  $m_{F555W} \sim 24.1$  mag, within the *Chandra* error circle of 1RXH J132519.8–430312 in *Hubble* images taken 195 days before the nearest X-ray observation. The optical brightness of this source is consistent with a late O or early B star at the distance of Cen A. If the optical source is the counterpart, then the X-ray and optical behavior of 1RXH J132519.8–430312 are similar to the transient Be/X-ray pulsar A 0538–66.

*Subject headings:* X-rays:individual(1RXH J132519.8–430312)–X-rays:binaries–galaxies:individual(Cen A)

---

<sup>1</sup>Universities Space Research Association, NASA Marshall Space Flight Center, XD12, Huntsville, AL, USA

<sup>2</sup>Space Science Department, NASA Marshall Space Flight Center, XD12, Huntsville, AL, USA

<sup>3</sup>MSSL, University College London, Holmbury St. Mary, Surrey, RH5 6NT, UK

## 1. Introduction

X-ray transients in our Galaxy and the Magellanic clouds have been observed since the beginning of X-ray astronomy. In systems with low-mass stellar companions, accretion is generally through an accretion disk which is fed by Roche lobe overflow of the companion. The transient outbursts are believed to be due either to an instability in the accretion disk similar to the thermal-viscous instability which causes dwarf nova outbursts in cataclysmic variables (van Paradijs 1996), or to an instability in the companion’s mass loss due to heating of its atmosphere by radiation from the X-ray source (Hameury et al. 1986). Many of these soft X-ray transient (SXT) outbursts are extremely bright, with one of the most luminous that from SAX J1819.3-2525 (V4641 Sgr) which reached an X-ray luminosity of  $\sim 6 \times 10^{39}$  ergs  $s^{-1}$ , or  $\sim 7$  times the Eddington luminosity for this  $7 M_{\odot}$  black hole (McClintock & Remillard 2003).

High-mass X-ray binary transient sources, on the other hand, are normally Be/X-ray binaries in which a high magnetic field neutron star accretes from the circumstellar outflow of the Be star (Verbunt & van den Heuvel 1995). There are two forms of outburst: type I which occur near periastron passage in wide eccentric orbit systems, tend to recur for a number of orbits in sequence, and reach luminosities of  $10^{35-37}$  ergs  $s^{-1}$ ; and type II which occur singly, may last for multiple orbits, and often reach the Eddington luminosity (Negueruela 1998). The most luminous observed outburst was from A 0538–66 (1A 0535–668) which reach a peak luminosity of  $L_x = 8.5 \times 10^{38}$  ergs  $s^{-1}$  in the 2-17 keV band (White & Carpenter 1978).

Identifying luminous transients in other galaxies is rare because of source confusion within the host galaxy, the infrequency of X-ray observations of individual galaxies, and the relative faintness of even the brightest non-nuclear point sources in nearby galaxies. The transient 1RXH J132519.8–430312 discovered by Steinle, Dennerl & Englhauser (2000) in *ROSAT* images of Cen A (NGC 5128) is an exception: 1RXH J132519.8–430312 is in a relatively isolated region of Cen A away from the nucleus and the conspicuous dust lane, there have been numerous deep X-ray observations of Cen A, and Cen A is only 4 Mpc distant (Ferrarese et al. 2000; Hui et al. 1993). Previous analysis of the *ROSAT* observations of this source were reported by Steinle et al. (2000) and of a subset of the *Chandra* observations by Kraft et al. (2001).

In this paper we assemble the long-term X-ray light curve of 1RXH J132519.8–430312 spanning 1990 to 2003 (§ 2). Our analysis accounts for a weak nearby source visible in *Chandra* images (see also Kraft et al. 2001) that is unresolved in *ROSAT* and *XMM-Newton* observations. We use the high time resolution *ROSAT* and *Chandra*/High Resolution Camera (HRC) observations to search for coherent pulsations and describe our procedure and results in § 3. Analysis of available *Hubble* images is presented in § 4. We summarize our

analysis in § 5 and show that the data favor the interpretation of 1RXH J132519.8–430312 as an example of a Be/X-ray binary in Cen A like A 0538–66.

## 2. The 1990-2003 X-ray light curve of 1RXH J132519.8–430312

The chronology of X-ray observations of 1RXH J132519.8–430312 is presented in Table 1. We estimated the fluxes listed in Table 1 by scaling from the only observation made with moderate spectral resolution while the source was bright; the *Chandra*/ACIS-I observation of 1999 Dec 5 (Table 1). Figure 1 displays the 1999 Dec 5 spectrum and the best-fit model. Table 2 lists all the spectral models we applied, fit parameter values, and fit statistics. Except the `powerlaw` model, all trial models produced acceptable fits. The `cutoffpl` (`powerlaw * highecut`) or `diskbb` models produced the lowest  $\chi^2$  statistic. For all the other observations, we used the bremsstrahlung spectral fit parameters as inputs to PIMMS (Mukai 1993) to convert observed count rates to estimated fluxes in the 0.1–2.4 keV band.

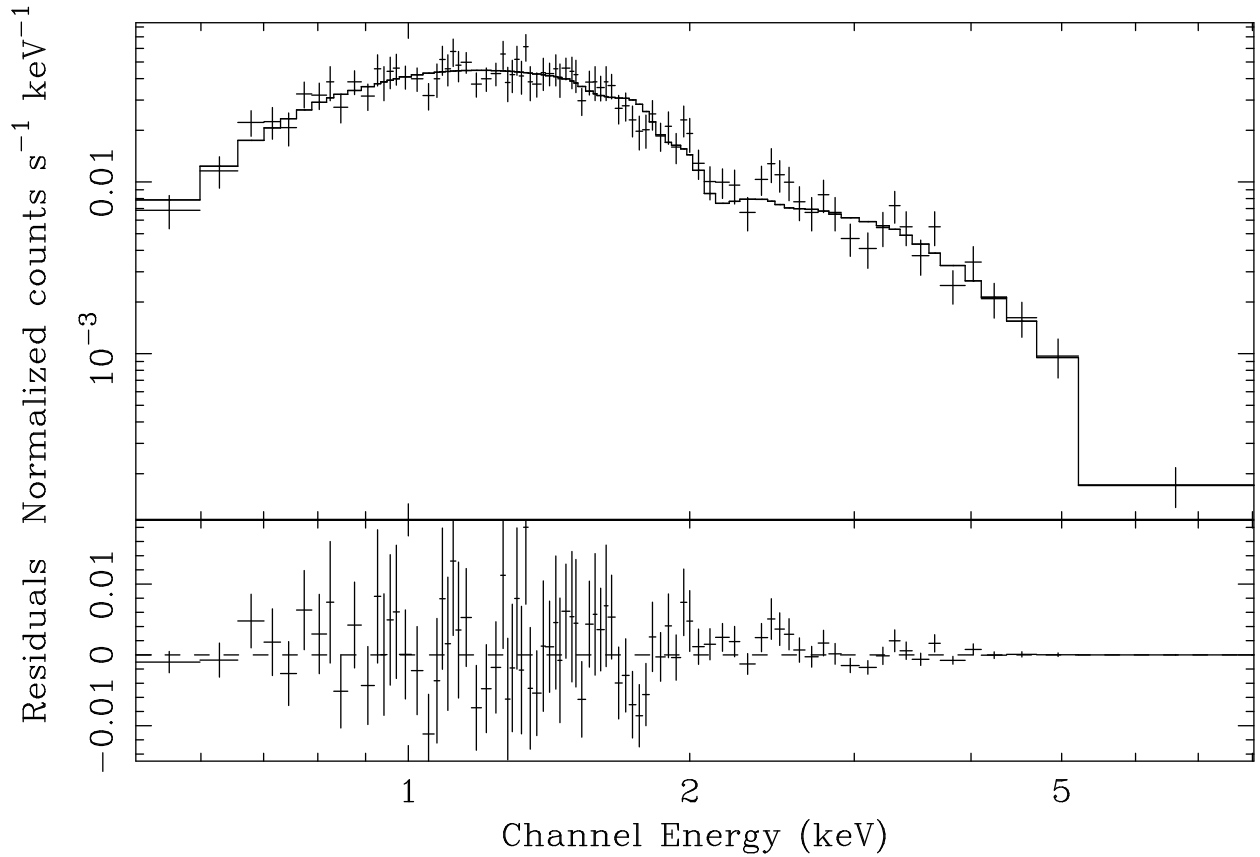
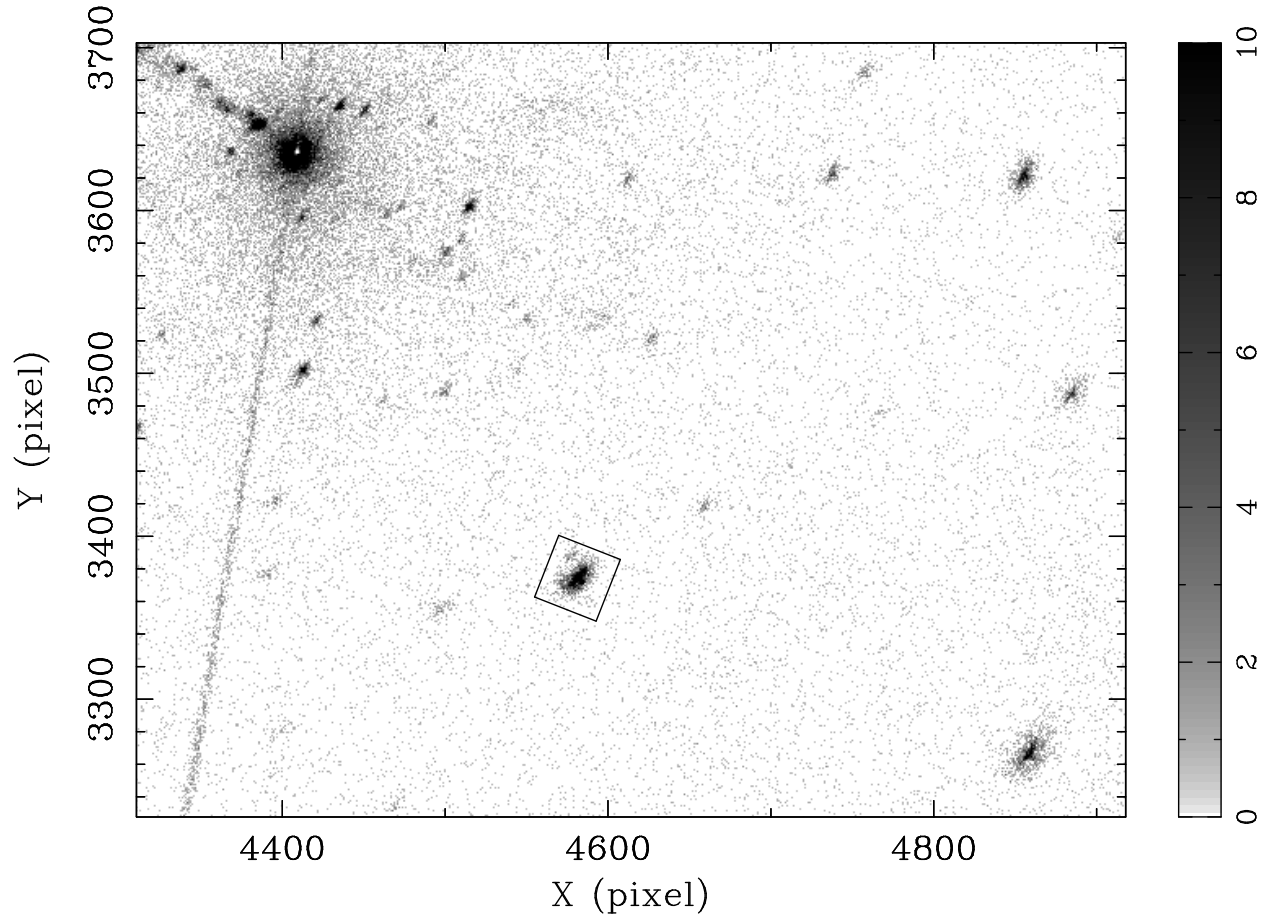


Fig. 1.— The *Chandra*/ACIS-I spectrum of 1RXH J132519.8–430312 obtained on 1999 December 05 is shown along with the best-fitting absorbed cut-off power law (powerlaw  $\times$  highcut) model and fit residuals. Parameter values and fit statistics for this and other trial models are listed in Table 2.

Figure 2 displays a portion of two *Chandra*/ACIS images of the Cen A field that illustrate the transient nature of 1RXH J132519.8–430312 and the presence of a weak nearby source. The weak source is CXOU J132520.1-430310 (Kraft et al. 2001). We estimated the flux from this source to be  $(8.6 \pm 1.1) \times 10^{-15}$  ergs cm $^{-2}$  s $^{-1}$  in the 2000 May 17 *Chandra*/ACIS-I observation.

Our re-analysis of *ROSAT* data (*cf.* Steinle, Dennerl & Englhauser 2000) took advantage of the precise *Chandra* location of 1RXH J132519.8–430312 relative to the nearby bright object H13 ( Fig. 2; see also Turner et al. 1997). Using this offset, we then extracted the counts from a circular region of 30'' radius centered at the transient position in the *ROSAT* images and subtracted a background determined from a circular annulus extending from 30'' to 60'' radii, also centered at the source position. Our resulting flux values are systematically lower than those obtained by Steinle, Dennerl & Englhauser (2000) primarily because they assumed a power law with  $\Gamma = 1.5$  and intervening absorption column of  $N_{\text{H}} = 8 \times 10^{20}$  cm $^{-2}$ , in their derivation in contrast to our bremsstrahlung model (Table 2). A marginal detection in the 1994 August 10 observation was attributed to the weak nearby source seen by *Chandra*.



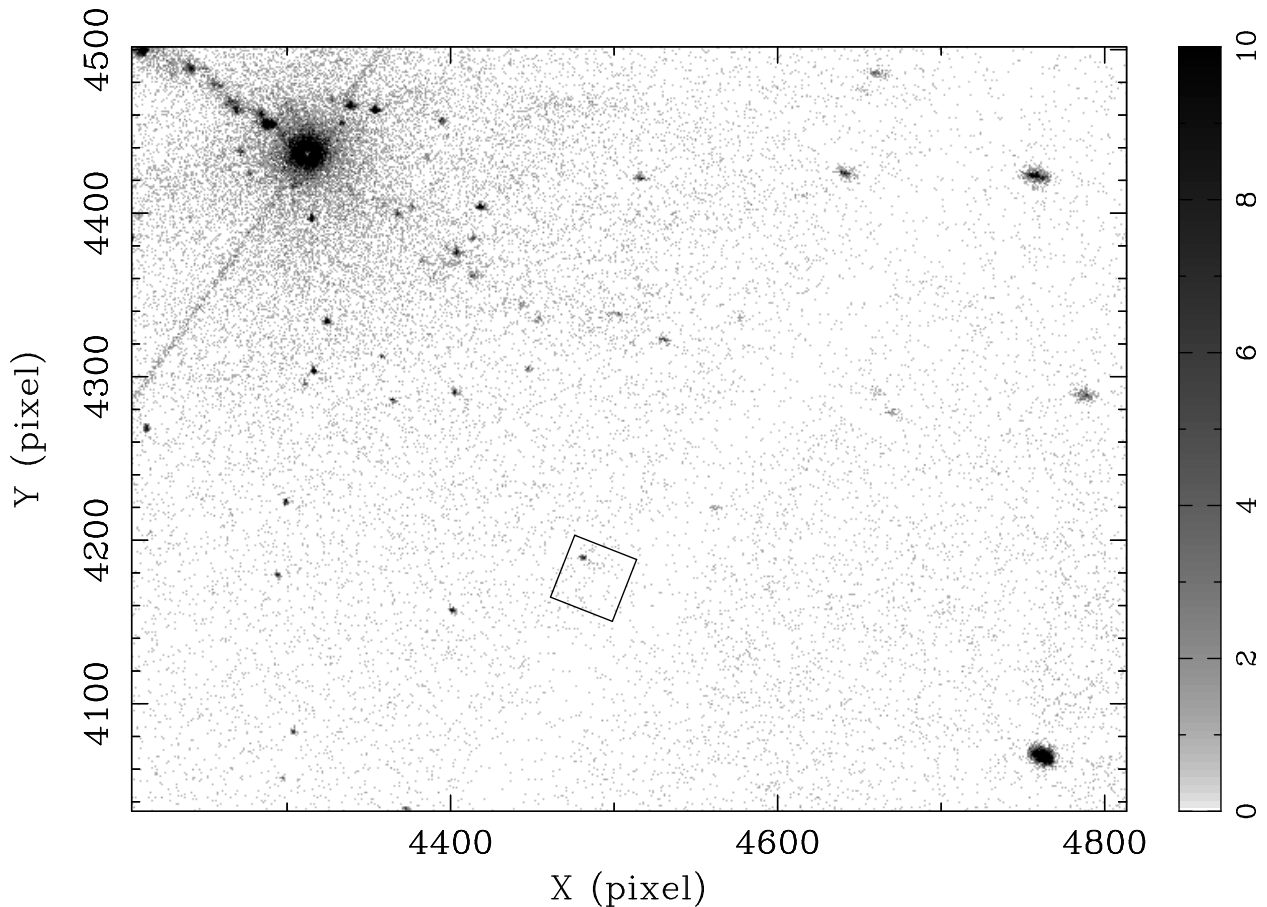


Fig. 2.—  $6.4 \times 4.0$  portions of *Chandra*/ACIS-I observations of Cen A obtained on 1999 December 5 (*top*) and 2000 May 17 (*bottom*). North is up and east is to the left. The  $20'' \times 20''$  box centered on 1RXH J132519.8–430312 represents the HST field displayed in Figure 8. There is a nearby weak source, CXOU J132520.1-430310, visible most clearly in the latter image within the box. This source is blended with 1RXH J132519.8–430312 in lower-resolution *ROSAT* and *XMM-Newton* observations. Note the readout streak from the bright Cen A nucleus indicating the spacecraft roll angle change. The bright object at the lower right hand corner of each image is H13 (Turner et al. 1997), which was used to precisely determine the location of 1RXH J132519.8–430312 in *ROSAT* and *XMM-Newton* observations.

For the *Chandra* observations, we extracted counts from an ellipse of half width  $9''$  and half height  $6''$  with a position angle dependent on the spacecraft roll at the time of observation. Corresponding background counts were extracted from the same size ellipse centered at three different positions around the transient and then averaged. For the ACIS/HETG observations, only the zeroth-order images were analyzed.

For the *XMM-Newton* observations, we used *XMM-Newton* Science Analysis System - GUI version 1.52.7 to process the EPIC MOS and pn images. The position of the transient was determined with respect to the precise location of H13 (Turner et al. 1997). Counts from the source and the background were extracted from a circle of radius  $10''$  and a circular annulus of  $10''$  and  $20''$  radii, respectively, at the position of 1RXH J132519.8–430312 in the 0.2 – 10 keV band.

We show in Figure 3 the combined 0.1–2.4 keV light curve of 1RXH J132519.8–430312. The source was bright during a 10 day period in 1995 July and in two observations separated by 16 days in 1999 December (see also Table 1). Three months prior to the 1999 December observations, the source was detected but at less than 10% of the flux it attained in 1999 December. The source faded to below the detection threshold in all subsequent observations except during the 2001 May 21 ACIS/HETG observation where the source was detected at a flux of only  $3.5 \times 10^{-15}$  ergs cm $^{-2}$  s $^{-1}$ . For non-detections, we show  $2\sigma$  upper limits in Table 1 and Figure 3.

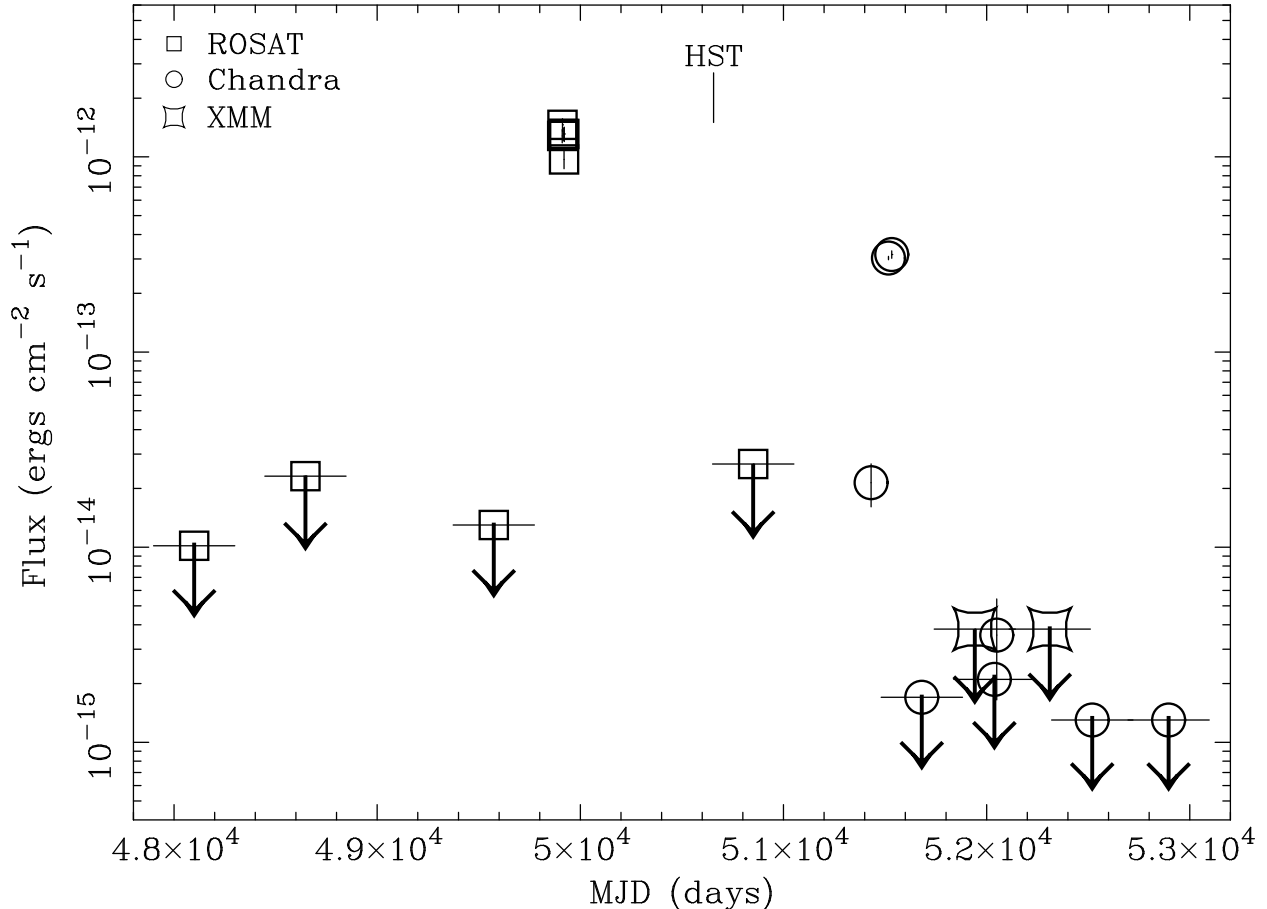


Fig. 3.— The 0.1–2.4 keV light curve of 1RXH J132519.8–430312 between 1990 and 2003 is shown. The horizontal bars above the data points indicate upper-limits. The vertical line below “HST” indicates the epoch of the HST observation described in § 3.

### 3. Short-term variability

Transient black-hole binaries and transient Be/X-ray binaries both show short term (ms to ks) variability. In black-hole systems the strength of aperiodic variability and the shape of the power-spectra are strongly dependent on the spectral state (McClintock & Remillard 2003). During the giant outbursts of Be/X-ray pulsars the broad band aperiodic variability is often stronger than the pulsations, with strong low-frequency quasi-periodic oscillations often appearing in the power spectra (Finger 2004). It is therefore of interest to quantify the short term aperiodic variability of 1RXH J132519.8–430312 and to search for coherent



pulsations.

We constructed short-term light curves of 1RXH J132519.8–430312 spanning individual observations and using the same extraction regions as described above to look for variability on short timescales. For example, the light curve during the 1999 December 5 *Chandra*/ACIS-I observation is shown in Figure 4. A total of 2264 counts were obtained in the 0.2–10.0 keV energy range, which were binned into 73 intervals of 500 s width. The light curve was steady during this observation according to a  $\chi^2$  test against the constant count rate hypothesis (reduced  $\chi^2=0.995$ ). Figure 5 displays the *Chandra*/HRC light curve on 1999 September 10. Again using 500 s bins, the unweighted average is 1.4 counts per bin. A  $\sim 1500$  s flare occurred at the beginning of the observation, lasted through three consecutive bins, and contained a total of thirteen photons. A Monte Carlo simulation of a constant source with Poisson noise showed a probability of  $6.0 \times 10^{-3}$  for two successive bins in the light curve with a total of more than ten photons making it unlikely that this flickering is a statistical fluctuation. The light curves during the other observations are similar to these examples: A steady flux when 1RXH J132519.8–430312 is at its brightest and flickering during fainter episodes.

A power-spectrum analysis was conducted using event data from the 1999 December 5 *Chandra*/ACIS-I observation, but no excess power above the Poisson noise was detected. The upper limit ( $2\sigma$ ) to a constant power spectra in the  $3 \times 10^{-5} - 0.154$  Hz frequency range is  $0.5 (\text{rms}/\text{mean})^2 \text{ Hz}^{-1}$  at  $10^{-3}$  Hz. The upper limit for a zero-frequency Lorentzian with half-power cutoff at  $10^{-2}$  Hz is  $2.6 (\text{rms}/\text{mean})^2 \text{ Hz}^{-1}$  at  $10^{-3}$  Hz.

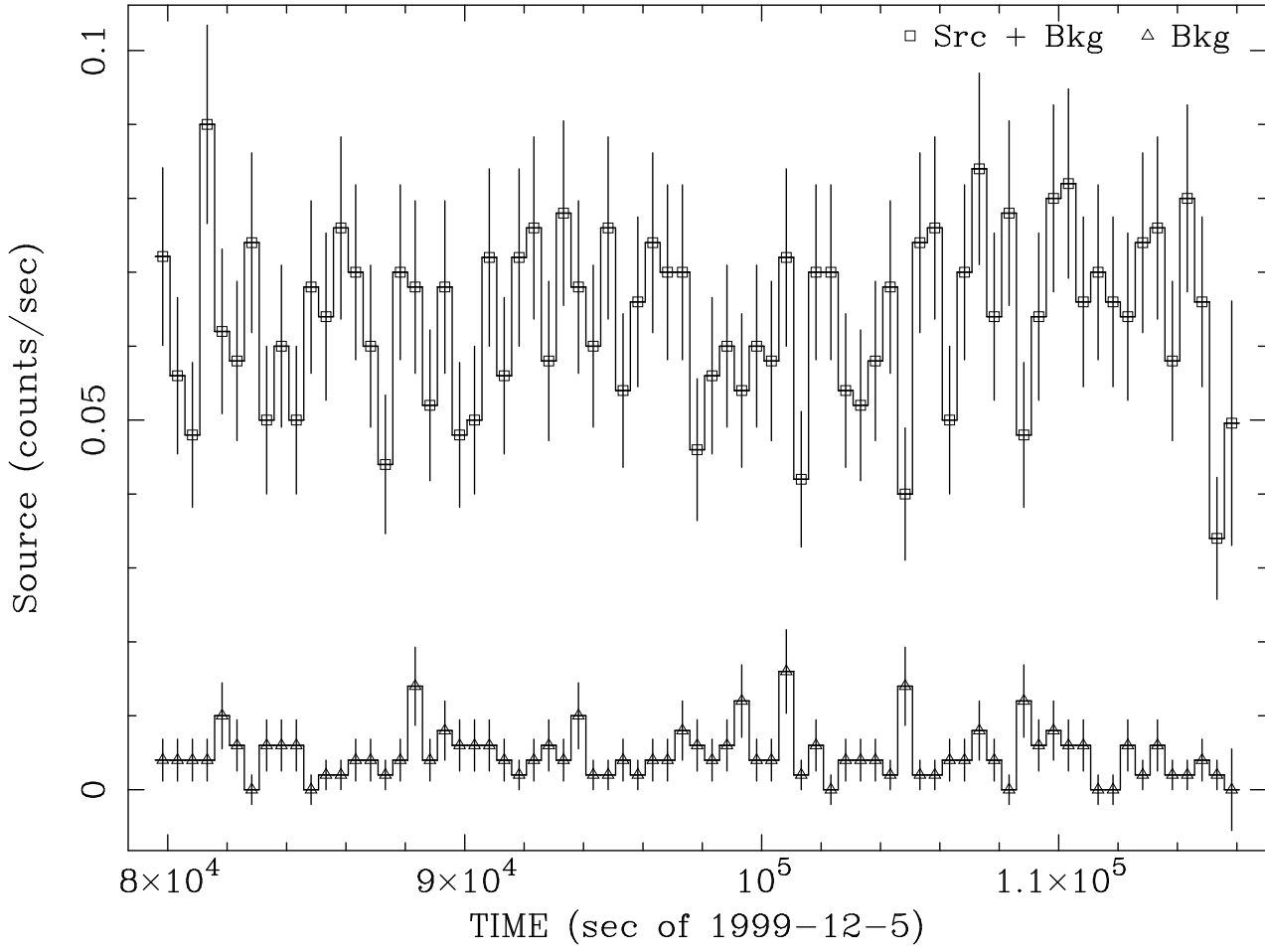


Fig. 4.— The 0.2–10.0 keV light curve of 1RXH J132519.8–430312 during the *Chandra*/ACIS-I observation of 1999 December 05. The source was bright and steady. Counts were binned into 500 s intervals.

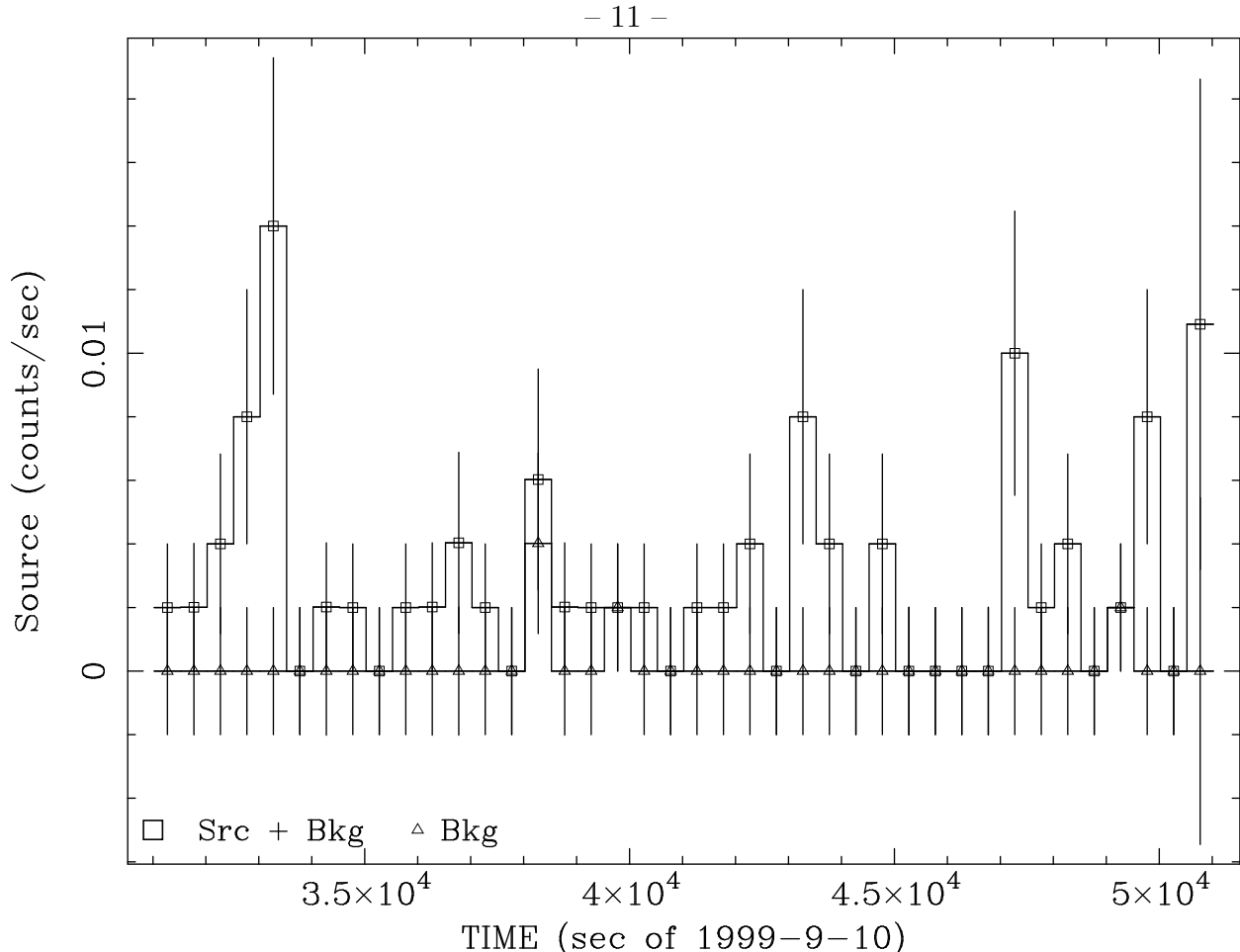


Fig. 5.— The full-band light curve of 1RXH J132519.8–430312 during the *Chandra*/HRC-I observation of 1999 September 10. The average source flux is about 10% of the average on 1999 December 05 (*cf.* Figure 4). Counts were binned into 500 s intervals.

A search for coherent pulsations in the  $3 \times 10^{-5}$  to 0.154 Hz frequency range was made in the 1999 December 5 *Chandra*/ACIS-I data, but none were detected. The search used the  $Z_n^2$  statistics (Buccheri et al. 1983) with both  $n = 1$  and  $n = 2$  Fourier terms. The arrival times used were referred to the solar-system barycenter using the *ciao* tool `axbary` with the DE200 planetary ephemeris. We obtained a 90% confidence upper limit of 12% on the rms pulse fraction. The maximum values of  $Z_n^2$  are consistent with Poisson statistics. (We note that this applies to simple pulse profiles limited to at most two Fourier terms.)

A search for coherent pulsations with frequency up to 20 Hz was made in the 1999 December 21 *Chandra* HRC-I data. Figure 6 shows the  $Z_2^2$  statistic calculated from the 481 barycenter-corrected events extracted from a  $6''$  by  $3''$  ellipse centered on the source.

The peak value was 47.39 at a barycentric frequency of 13.264391(3) Hz. To estimate the significance, we used a Monte Carlo algorithm to generate 33800 simulated data sets of 481

events each. Forty-seven of these data sets had peaks exceeding 47.39 in the 0–20 Hz range indicating the probability of seeing such a peak in any one spectrum is  $(1.4 \pm 0.2) \times 10^{-3}$ . To test for instrumental effects, we also tested 635 background regions extracted from the HRC-I data, each containing 481 events, and found two with peaks above 47.39 for a probability of  $(3.2 \pm 2.2) \times 10^{-3}$ .

In Figure 7 we show the epoch-folded pulse profile, which has an rms pulse fraction of 31% (two Fourier terms). The amplitude of the pulsations is only marginally increased by including a frequency rate term in the analysis. We measure a frequency rate of  $(-2.4 \pm 1.6) \times 10^{-9} \text{ Hz s}^{-1}$ .

We were unable to confirm these pulsations using the *ROSAT*/HRI data from 1995 July. These data, which consists of 820 events (37 being background), are spread non-uniformly over an interval of 10 days. These data are therefore very sensitive to small changes in frequency and therefore require a search in both frequency and frequency-rate with a large number of trial parameters. We used the  $Z_2^2$  statistic to search for pulsations at a frequency within 55 mHz of the Chandra HRC-I detection, and frequency rate in the range of  $-5.5 \times 10^{-9}$  to  $5.5 \times 10^{-9} \text{ Hz s}^{-1}$ . The arrival times used were referred to the barycenter using the *ROSAT* FT00LS `bct` and `abc`. We find an upper limit of 27% for any pulsations in this parameter range. If pulsations were present with the same pulse fraction as seen in the Chandra data, with pulse phasing that could be accurately described by a frequency and frequency rate in the search range, then it would have been clearly detected. The lack of detection could be due to a decrease of pulse fraction with decreasing energy, or the narrowness of the ranges of frequency and frequency-rate which was covered, which were limited by the amount of computation involved ( $2^{10}$  evaluations of  $Z_2^2$ ). In particular we point out that we failed to cover the frequency rate of  $-1.0 \times 10^{-7} \text{ Hz s}^{-1}$  observed for A 0538–66, and that the occurrence of a strong orbital modulation (i.e. periastron passage) within the data interval would have prevented detection.

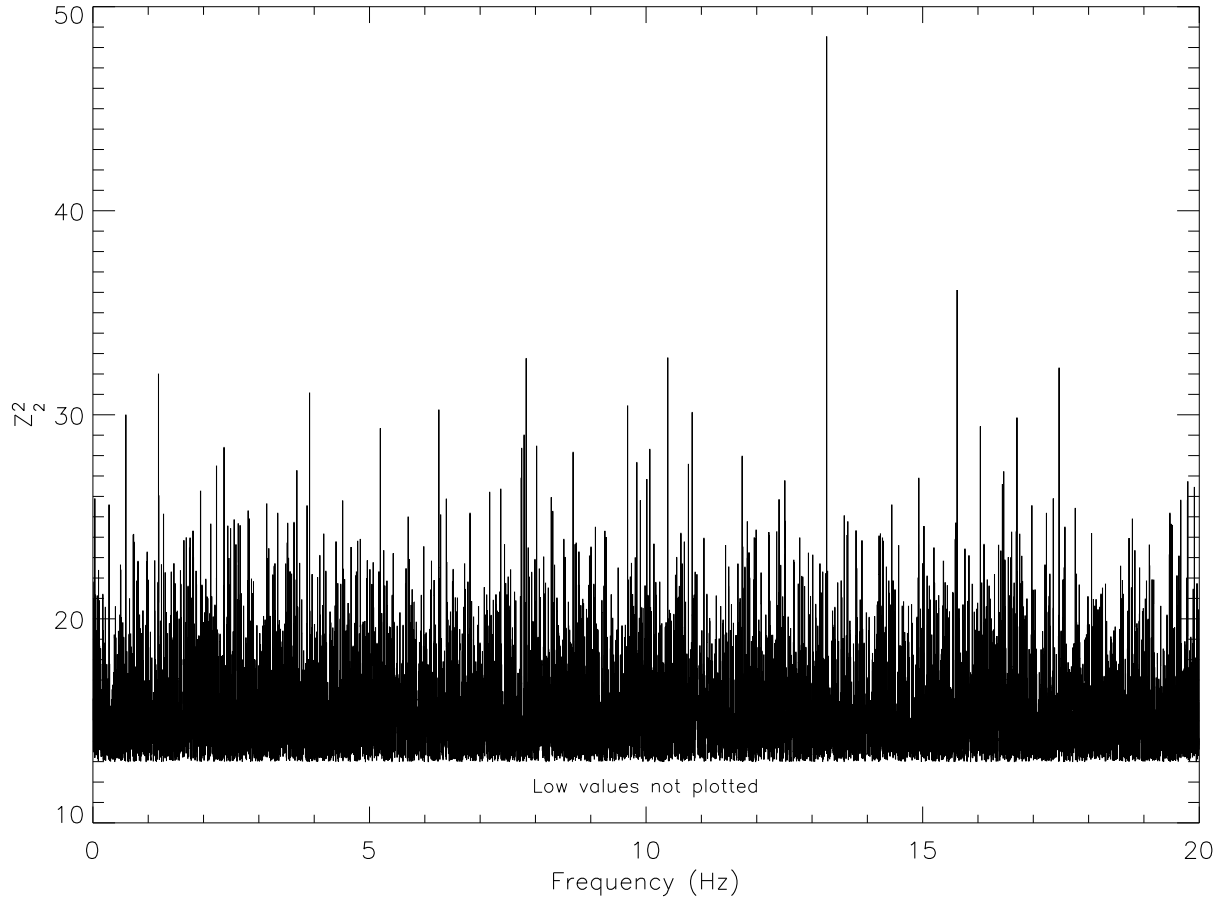


Fig. 6.— The  $Z_2^2$  pulse search statistic for the Chandra/HRC-I data of 1999 December 12 showing a significant peak at 13.264391 Hz.

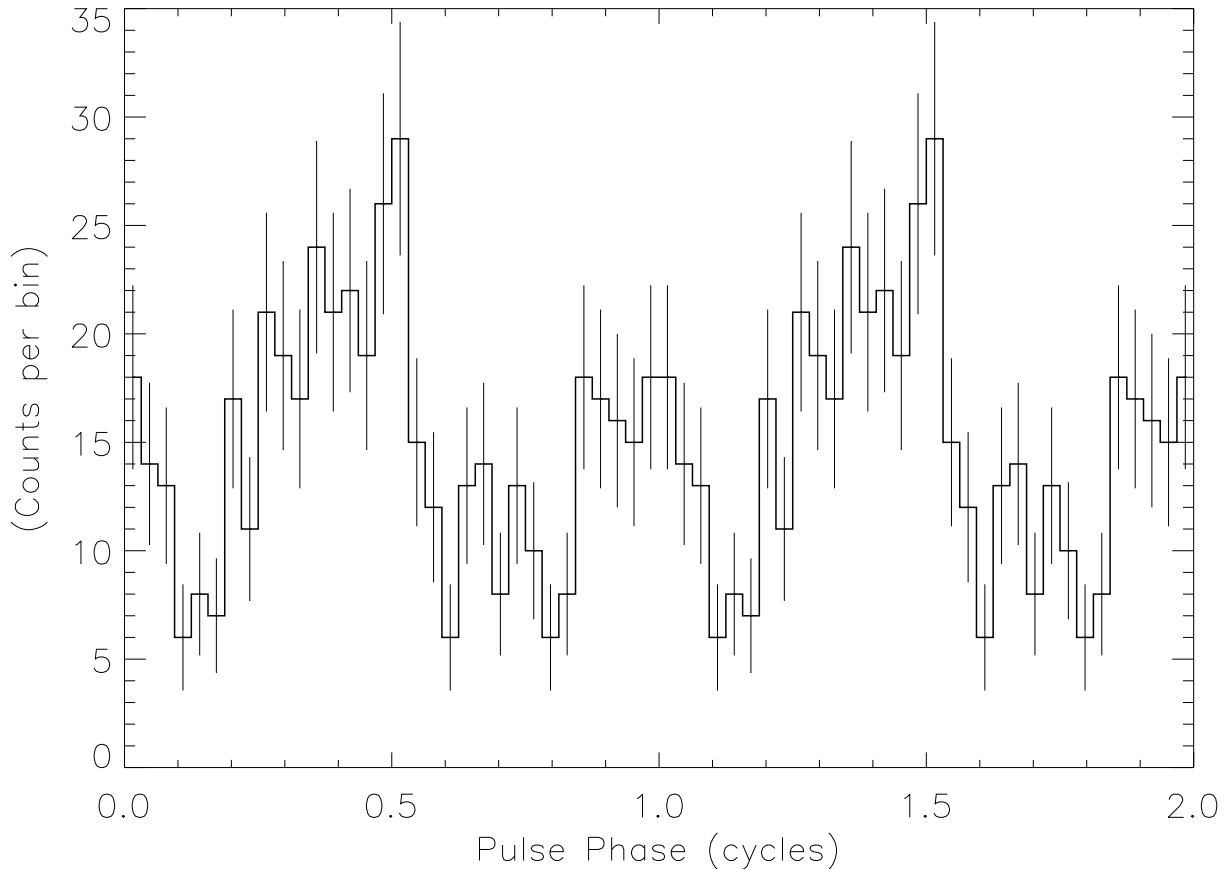


Fig. 7.— Epoch-folded pulse profile of the Chandra/HRC-I lightcurve of 1RXH J132519.8–430312 obtained on 1999 December 12.

#### 4. An Optical Counterpart Candidate

There are two *Hubble* Space Telescope observations with 1RXH J132519.8–430312 in the field of view. These observations were taken in 1997 July 27 (MJD = 50656; 195 days before the nearest X-ray observation on 1998 Feb 7, see Table 1). The observations used the Wide Field Planetary Camera 2 (WFPC2) with the F555W and F814W filters, respectively. Both consisted of three 60 s exposures that were combined to remove cosmic ray tracks.

We first located the globular cluster HGHH-06 (Harris et al. 1992; Peng et al. 2004) in the HST image, which gives an approximate correction to the HST coordinates. With this correction, the Chandra source CXOU J132520.1-430310 (Kraft et al. 2001) lies very close to the bright object near pixel location (443, 594) shown in Fig. 8. If we assume

that this source is the optical counterpart to CXOU J132520.1-430310, we can then derive a relative HST/Chandra coordinate offset. The offset in R.A. and Dec. of the catalogued position of CXOU J132520.1-430310 from its position in the *Hubble* data is  $\Delta\alpha = -0.22$  s and  $\Delta\delta = +1.7''$ . We applied this offset to register the *Hubble* and *Chandra* images.

Figure 8 shows a  $20'' \times 20''$  region of the *Hubble* F555W image centered at the expected position of 1RXH J132519.8–430312 with the 90% confidence level *Chandra* error circle marked. There is an object within this error circle. Its observed magnitudes are  $24.1 \pm 0.6$  and  $23.1 \pm 0.6$  in the F555W and F814W images, respectively. The probabilities of finding a source of similar brightness in these two images due to statistical fluctuation alone are 1% and 7%, respectively. By fitting a 2D circular Gaussian to both the F555W and F814W data we find the position differs, at the 90 percent confidence level, by 1.5 pixel ( $\sim 0.15$  arcsec). This relative offset could be due to the blending of two objects in the F814W image.

Correcting for Galactic extinction yields an absolute magnitude  $M_{F555W} = -4.5 \pm 0.6$  mag and a color  $(F555W-F814W) < 0.7 \pm 0.8$  mag. The absolute magnitude is consistent with that of a late O or early B main-sequence star. The extinction-corrected color is redder than that of main-sequence O and B stars (*cf.*  $V-I = -0.4$  for a B0 star). The observed color could be made consistent with that of an OB star if  $\sim 2/3$  of the flux measured in the F814W image is due to an unrelated second source.

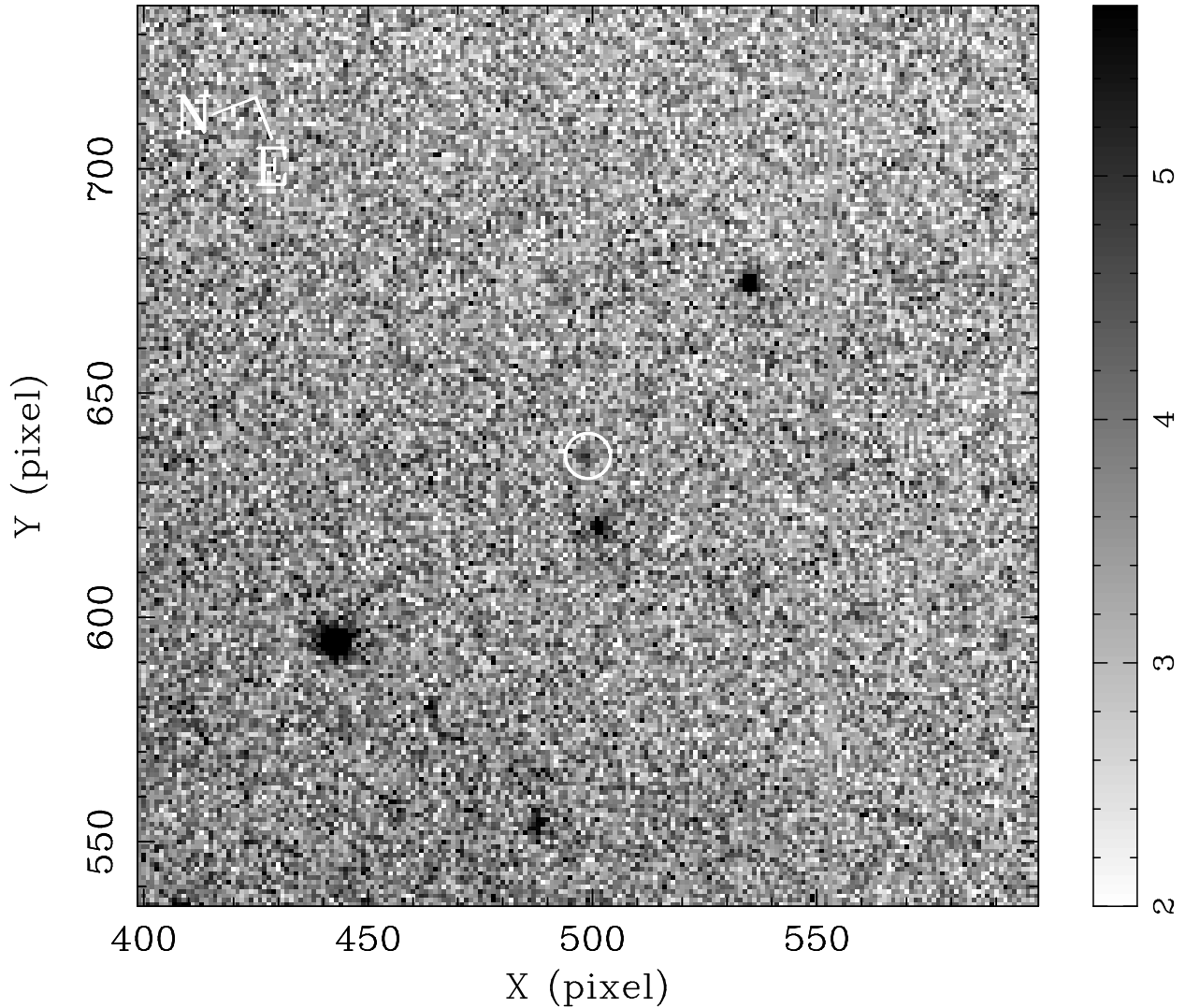


Fig. 8.— A  $20'' \times 20''$  portion of the *Hubble*/F555W image of Cen A centered on the position of 1RXH J132519.8–430312. The (true)  $0.48''$  *Chandra* error circle is shown at the astrometrically-corrected position of the transient. North and East are indicated at upper left.

### 5. The nature of 1RXH J132519.8–430312

The inferred isotropic luminosity of 1RXH J132519.8 –430312 peaked above  $10^{39}$  ergs  $s^{-1}$  during two episodes separated by a 4.4 year interval within a 13 year observing span. This places 1RXH J132519.8–430312 at the low end of the distribution of luminosities observed



among the class of ultra-luminous X-ray sources (Fabbiano 1989; Swartz et al. 2004) and in the realm of luminous outbursts observed from several well-studied Galactic and Magellanic Cloud X-ray sources (Liu, van Paradijs & van den Heuvel 2000, 2001); primarily the (high-mass) Be/X-ray binaries and the (usually low-mass) SXTs.

Many of the characteristics of 1RXH J132519.8 –430312 presented here can be explained by comparison to either of these classes of Galactic systems: 1RXH J132519.8–430312 varied in flux by at least a factor of 1000 consistent with the range observed for both Be/X-ray binaries and SXTs (which can be  $\sim 10^6$  corresponding to quiescent flux levels far below detectability of 1RXH J132519.8–430312). The spacing and duration of outbursts of 1RXH J132519.8–430312 are not well constrained because of the sparsely scheduled observations, but the interval of 4.4 years between observed outbursts and the  $\sim 2$  week outburst durations are within the range of timescales observed in the Galactic Be/X-ray binaries and SXTs. The peak luminosity of 1RXH J132519.8–430312 is in the range observed for black hole SXTs and within a factor of a few of the most luminous Be/X-ray binary A 0538–66. The spectrum during the peak luminosity episode of 1RXH J132519.8–430312 is represented equally well by either a disk blackbody model like the high/soft or very high/soft state spectra of SXTs or a cut-off powerlaw of accreting pulsars<sup>1</sup>. Note that, due to the low number of photons detected, the observations of 1RXH J132519.8–430312 cannot be used to detect the more moderate aperiodic behavior in the  $10^{-2}$  Hz and higher range typically seen in SXTs and in giant outbursts of Be/X-ray binaries although violent variability at low frequencies can be detected.

Two characteristics of 1RXH J132519.8–430312 can best be explained only in analogy to the Be/X-ray binaries. The detection of a potential optical companion to 1RXH J132519.8–430312 with the brightness of a late O or early B star is just what is expected for a Be/X-ray binary. For example, the companion of A 0538–66 is a B2 III-IV star (Charles et al. 1983) and would appear to be 23.9 mag if it was in Cen A. More importantly, the coherent pulsations we have detected in 1RXH J132519.8–430312 can only be explained in conjunction with a spinning magnetized neutron star. In fact, the period of 75.4 ms is remarkably similar to the 69.2 ms period of A 0538–66 (Skinner et al. 1982). This identification could be made more definitive if optical variability (preferably correlated with changes in X-ray flux) could be established and if the X-ray pulsations could be confirmed with another outburst observation (preferably with *XMM-Newton* to also obtain another X-ray spectrum).

In many aspects, we cannot consider 1RXH J132519.8 –430312 as a perfect analog

---

<sup>1</sup>Low cut-off energies have also been observed in the Be/X-ray binaries BSD 24–491 (Reig & Roche 1999); X Per (Schlegel et al. 1993); LSI +61235 (Haberl, Angelini & Motch 1998).

to A 0536–66. This source reached a luminosity of  $8.5 \times 10^{38}$  ergs  $s^{-1}$  for only a few hours, during an outburst that lasted a few days. A later super-Eddington outburst, lasted for 2 weeks, but showed an  $\sim 4$  day e-folding decay (Skinner et al. 1980). In contrast, 1RXH J132519.8–430312 was surprisingly constant for 10 days in the ROSAT outburst. However, A 0538-66 does provide an example of a neutron star radiating far above the Eddington luminosity. Indeed, at the base of the accretion column the accretion rate per unit area must be super-Eddington by a factor approaching two orders of magnitude.

It is the magnetic field of the pulsar which produces an efficient segregation of mass inflow and photon outflow that allows such super-Eddington conditions to exist. The observations can be used to place constraints on the neutron star’s magnetic field. The magnetic field must be strong enough to channel the accretion flow near the stellar surface. For a  $1.4 M_{\odot}$  neutron star of radius  $10^6$  cm, a polar strength greater than  $6 \times 10^8$  G for a dipole magnetic field is needed to maintain the magnetosphere above the neutron star surface when the accretion rate is sufficient to produce a luminosity of  $10^{39}$  ergs  $s^{-1}$ . At low accretion rates, the magnetosphere can expand beyond the radius at which a Keplerian orbit co-rotates with the neutron star resulting in material embedded in the field being flung off by centrifugal forces. In this “propeller regime,” accretion to the surface is inhibited (Stella, White & Rosner 1983). Reduced levels of X-ray emission may occur due either to leakage through the lower centrifugal barrier near the spin axis, or due to accretion onto the magnetosphere (King & Cominsky 1994). The transition to this regime occurs at a luminosity

$$L_{\text{transition}} = 4 \times 10^{37} M_{1.4}^{-2/3} R_6^5 B_{12}^2 \nu_{Hz}^{7/3} \text{ ergs } s^{-1}$$

where  $M_{1.4}$  is the mass of the neutron star in units of  $1.4 M_{\odot}$ ,  $R_6$  its radius in units of  $10^6$  cm,  $B_{12}$  its polar field in units of  $10^{12}$  G, and  $\nu_{Hz}$  its spin frequency in Hz. The flaring during the 1999 Sept 10 HRC-I observations could be explained by the unstable accretion expected during the transition to the propeller regime (Spruit & Taam, 1993). This would imply  $B \approx 6 \times 10^{10}$  G for a  $1.4 M_{\odot}$  neutron star and  $10^6$  cm radius.

1RXH J132519.8–430312 is classified as an ultraluminous X-ray source by virtue of its peak luminosity. How does 1RXH J132519.8–430312 compare to the general class of ULXs? During its peak brightness episodes, the X-ray properties of 1RXH J132519.8–430312 are within the broad range of values observed from other ULXs. For example, 30% of the ULXs surveyed by Swartz et al. (2004) have power law indices between 2.0 and 3.0 (although the average of the whole sample is only 1.7) and 86% showed no significant variability during times of observation. However, the fraction of ULXs that are *transient* has not yet been documented so we do not know how common this characteristic of 1RXH J132519.8–430312 is among the general class of ULXs. There have also been several reports of late O or

early B star companions to ULXs (e.g. Liu et al. 2005) like the candidate counterpart to 1RXH J132519.8–430312.

How common could Be/X-ray binaries like 1RXH J132519.8–430312 be within the ULX population? A large number of Be-type binary systems is expected in typical galaxies with modest star formation rates. For example, the population synthesis studies of Dalton & Sarazin (1995) predict  $>20000$  potential Be-type binary systems exist in our Galaxy based on the observed Lyman continuum flux. In fact, most of the 130 known high-mass X-ray binaries in the Galaxy and Magellanic Clouds are Be/X-ray binaries (Liu et al. 2000). In addition, there is a strong correlation between ULXs and recent star formation in late-type galaxies. Be/X-ray binaries are short lived and they are expected to be found in young stellar environments such as those in late-type and interacting galaxies. Thus, the potential certainly exists for Be/X-ray binaries to make a significant contribution to the ULX population, at least at the low luminosity end, and the ULX 1RXH J132519.8–430312 may be the first such example.

Our sincere thanks to the anonymous referee for valuable comments that helped to improve the paper. This research has made use of the NASA/IPAC Extragalactic Database (NED) which is operated by the Jet Propulsion Laboratory, California Institute of Technology, under contract with NASA; of data products from the Two Micron All Sky Survey, which is a joint project of the University of Massachusetts and the Infrared Processing and Analysis Center, funded by NASA and the NSF; from the Multimission Archive (MAST) at the STScI operated by AURA under NASA contract NAS5-26555; and from the Chandra Data Archive, part of the Chandra X-Ray Observatory Science Center (CXC) which is operated for NASA by SAO. Support for this research was provided in part by NASA under Grant NNG04GC86G issued through the Office of Space Science.

## REFERENCES

- Bradt, H.V.D. and McClintock, J.E. 1983, ARAA 21, 13
- Buccheri, R. et al., 1983, A&A 128, 245
- Charles, P. A., et al. 1983, MNRAS, 202, 657
- Corbet, R. H. D. 1986, MNRAS, 220, 1047
- Dalton, W. W. & Sarazin, C. L. 1995, ApJ, 440, 280

- Ferrarese, L. et al., 2000, ApJS, 128, 421
- Finger, M. H., 2004, in “X-Ray Timing 2003”, API Conf. Proc. 714, P. Kaaret, F.K. Lamb, J. H. Swank ed., (API: Melville, New York), 342
- Haberl, F., Angelini, L. & Motch, C. 1998, A&A, 335, 587
- Harris, G. L. H., Geisler, D., Harris, H. C. & Hesser, J. E., 1992, AJ, 104, 613
- Helfand, D. J. & Moran, E. C. 2001, ApJ, 554, 27
- Hui, X., Ford, H., Ciardullo, R. & Jacobi, G. H., 1993, ApJ, 414, 463
- King, A. & Cominsky, L. ApJ 435, 411
- King, A. R. 2003, ApJL, 596, 27
- Kraft, R. P., Kregenow, J. M., Forman, W. R., Jones, C. & Murray, S. S., 2001, ApJ, 560, 675
- Liu, J.-F., Bregman, J. N., Seitzer, P., & Irwin, J. 2005, astro-ph/0501310
- Liu, Q. Z., van Paradijs, J., & van den Heuvel, E. P. J. 2000, A&ASS, 147, 25
- Liu, Q. Z., van Paradijs, J., & van den Heuvel, E. P. J. 2001, A&A, 368, 102
- McClintock, J. E. & Remillard, R. A., 2003, astro-ph/0306213
- Mukai, K. 1993, Legacy, 3, 21
- Negueruela, I. 1998, A&A 338, 505
- Negueruela, I. 2004, astro-ph/0411335
- Peng E. W., et al. 2002, AJ, 124, 3144
- Peng, E. W., Ford H. C. & Freeman K. C., 2004, ApJS, 150, 367
- Reig, P. & Roche, P. 1999, MNRAS, 306, 100
- Schlegel, E. M. et al. 1993, ApJ, 407, 744
- Skinner, G. K., Shulman, S., Share, G. et al., 1980, ApJ, 240
- Skinner, G. K., Bedford, D. K., Elsner, R. F., Leahy, D., Weisskopf, M. C., & Grindlay, J. 1982, Nature 297, 568

- Sputit, H. C. & Taam R. E. 1993, ApJ, 402, 593
- Steinle, H., Dennerl, K. & Englhauser, J., 2000, A&A, 357, L60
- Stella, L., White, N. E., & Rosner R. 1983, ApJ 308, 669
- Sunyaev, R. A. & Titarchuk, L. G. 1980, A&A 86, 121
- Swartz, D. A., Ghosh, K. K., Tennant, A. F. & Wu, K., 2004, ApJS, 154, 519
- Turner, T. J. et al. 1997, ApJ, 475, 118
- van Paradijs, J. 1996, ApJ, 464, L64
- Verbunt, F., & van den Heuvel, E. P. J. 1995 in X-ray Binaries,
- White, N. E., & Carpenter, G. F. 1978, MNRAS, 183, 11P
- White, N. E., Swank, H. J. & Holt, S. S. 1983, ApJ, 270, 711
- White, N. E., Nagase, F. & Parmar, A. N. 1995, In: Lewin, W. H. G., van Paradij, J., & van den Heuvel, E. P. J. (eds.), X-ray Binaries, Cambridge University Press, p. 1

TABLE 1  
Log of ROSAT, Chandra and XMM–Newton X-ray observations of Cen A (NGC 5128)

Date of obs. (yy–mm–dd)	MJD (days)	ObsID	Satellite/Instrument	Exposure (ksec)	0.1–2.4 keV Flux ( $10^{-15}$ ergs cm $^{-2}$ s $^{-1}$ )
90–07–27	48099	150004	ROSAT/HRI	19.52	$< 10.0^a$
92–01–26	48647	700012	ROSAT/PSPC	13.48	$< 23.0^a$
94–08–10	49574	701571	ROSAT/HRI	64.11	$< 13.0^a$
95–07–13	49911	701924	ROSAT/HRI	4.90	$1280 \pm 100$
95–07–14	49912	701925	ROSAT/HRI	5.33	$1460 \pm 110$
95–07–18	49916	701926	ROSAT/HRI	5.72	$1310 \pm 100$
95–07–22	49920	701927	ROSAT/HRI	4.09	$970 \pm 100$
95–07–23	49921	701928	ROSAT/HRI	4.06	$1310 \pm 110$
98–02–07	50851	704206	ROSAT/HRI	17.22	$< 27.0^a$
99–09–10	51431	463	Chandra/HRC-I	19.51	$21.4 \pm 5.3$
99–09–10	51431	1253	Chandra/HRC-I	6.81	$14.3 \pm 8.5$
99–12–05	51517	316	Chandra/ACIS-I	35.72	$303.1 \pm 6.0$
99–12–21	51533	1412	Chandra/HRC-I	14.97	$316.0 \pm 14.0$
00–05–17	51681	962	Chandra/ACIS-I	36.50	$< 1.7^a$
01–02–02	51942	93650201	XMM–Newton/MOS	23.02	$< 3.8^a$
01–05–09	52038	1600	Chandra/ACIS-S/HETG	46.84	$< 2.1^a$
01–05–21	52050	1601	Chandra/ACIS-S/HETG	51.50	$3.5 \pm 1.9$
02–02–06	52311	93650301	XMM–Newton/MOS/PN	8.89	$< 3.8^a$
02–09–03	52520	2978	Chandra/ACIS-S	44.59	$< 1.3^a$
03–09–14	52896	3965	Chandra/ACIS-S	49.52	$< 1.3^a$

<sup>a</sup>The upper limit is at the  $2\sigma$  level.

TABLE 2  
X-ray spectral parameters of 1RXH J132519.8–430312 on 1999 December 5

XSPEC Model	$N_{\text{H}}$ ( $10^{20} \text{ cm}^{-2}$ )	$\Gamma$	$E_{\text{cut}}$ (keV)	$T_{\text{e,in}}$ (keV)	$L_{\text{X}}^a$ ( $10^{39} \text{ ergs s}^{-1}$ )	$\chi^2/\text{dof}$
Power-law	$35.0^{+5.0}_{-5.0}$	$2.63^{+0.13}_{-0.12}$	—	—	$1.61 \pm 0.11$	112.3/82
Bremsstrahlung	$18.9^{+3.4}_{-3.2}$	—	—	$2.33^{+0.25}_{-0.22}$	$1.20 \pm 0.10$	80.1/82
Raymond-Smith <sup>b</sup>	$18.9^{+3.3}_{-3.0}$	—	—	$2.32^{+0.24}_{-0.21}$	$1.17 \pm 0.09$	80.1/81
Mekal <sup>b</sup>	$19.0^{+3.7}_{-2.7}$	—	—	$2.34^{+0.21}_{-0.23}$	$1.18 \pm 0.09$	79.9/81
Disk blackbody	8.63	—	—	$0.93^{+0.04}_{-0.04}$	$1.09 \pm 0.08$	71.8/83
Cut-off powerlaw <sup>c</sup>	$21.7^{+6.7}_{-3.2}$	$2.01^{+0.22}_{-0.27}$	$3.31 \pm 0.35$	$1.87^{+0.73^d}_{-0.40}$	$1.14 \pm 0.16$	70.2/80

<sup>a</sup> Intrinsic isotropic luminosity in the 0.5–8.0 keV band.

<sup>b</sup>Elemental abundance is a free parameter which converges to  $Z=0$ .

<sup>c</sup> Powerlaw \* highecut model in XSPEC

<sup>d</sup> Folding energy in keV.